Available online at www.sciencedirect.com
ScienceDirect
C. R. Chimie 11 (2008) 818–833
COMPTES RENDUS CHIMIE
http://france.elsevier.com/direct/CRAS2C/

Account / Revue

Nickel–thiolate and iron–thiolate cyanocarbonyl complexes: Modeling the nickel and iron sites of [NiFe] hydrogenase

Tzung-Wen Chiou, Wen-Feng Liaw*

Department of Chemistry, National Tsing Hua University, Hsinchu 30043, Taiwan

Received 21 November 2007; accepted after revision 4 April 2008
Available online 23 May 2008

Abstract

During the past decade, structures and functions (catalytic mechanism) of [NiFe]/[Fe] hydrogenases have been established/proposed. Model compounds, various biophysical measurements and theoretical calculations have been lent to elucidate the structure and function (catalytic mechanism) of active sites of [NiFe]/[Fe] hydrogenases. In this manuscript, biomimetic model compounds, including iron(II)–thiolate cyanocarbonyls, nickel(III)–thiolates and nickel(II)–thiolate complexes with pendant thiol, are presented. ***To cite this article: T.-W. Chiou, W.-F. Liaw, C. R. Chimie 11 (2008).***

Keywords: Nickel–thiolates; Iron–thiolate cyanocarbonyl; Hydrogenases; Model compound

1. Introduction

The impressive synergism that has developed in the past few years between biophysical and synthetic inorganic chemists with regard to understanding the spectroscopic signals and functions of the $[(SR)_zFe(CO)_x(CN)_y]$ and $[Ni(Cys)_4]$ active sites in [Fe]/[NiFe] hydrogenases has highlighted the chemistry of iron–thiolate cyanocarbonyl and nickel–thiolate complexes [1–12]. The recent report of high-quality single-crystal X-ray structure of [Fe]-only hydrogenase from *Desulfovibrio desulfuricans* revealed that the active site contains a dinuclear iron(II)–thiolate with mixed CO and CN^- coordinated ligands (H cluster) bound to a [4Fe–4S] cubane cluster via cysteinate bridge, and also suggested that the unsaturated Fe center present in the H cluster of the enzyme can act as a binding site for the soft ligand H_2 [3]. A more CO/CN^--rich environment was also found for iron in the recently reported X-ray structure of [Fe] hydrogenase isolated from *Clostridium pasteurianum* (CpI) [4]. A schematic drawing of the active center of [Fe] hydrogenases as deduced from the crystallographic studies is shown in Fig. 1. Moreover, the infrared spectra of [Fe] hydrogenase from *Desulfovibrio vulgaris* concluded that the weak absorption bands for the CN^- ligand range from 2079 to 2106 cm^{-1}, and the broad strong absorption bands (ranging from 2016 to 1894 cm^{-1}) are assigned to the carbonyl stretching frequencies under the various redox states [5].

The X-ray crystallographic studies of the active-site structure of [NiFe] hydrogenases isolated from *Desulfovibrio gigas*, *Desulfovibrio vulgaris*, *Desulfovibrio fructosovorans*, and *Desulfovibrio desulfuricans* ATCC27774, in combination with infrared spectroscopy, revealed that the active site is composed of a heterobimetallic

* Corresponding author.
E-mail address: wfliaw@mx.nthu.edu.tw (W.-F. Liaw).

1631-0748/$ - see front matter © 2008 Académie des sciences. Published by Elsevier Masson SAS. All rights reserved.
doi:10.1016/j.crci.2008.04.003

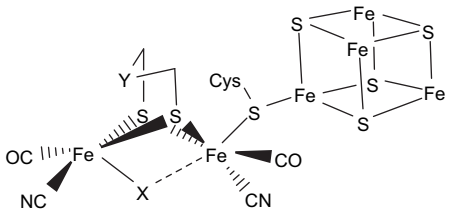

Fig. 1. Schematic drawing of the H cluster according to the X-ray crystal structure isolated from *D. desulfuricans* [Fe] hydrogenase (X = CO, H; Y = NH, CH_2) [3,4].

$(S_{cys})_2Ni(\mu\text{-}S_{cys})_2(\mu\text{-}X)Fe(CO)(CN)_2$ ($X = O^{2-}$, HO_2^-, OH^-) cluster (Fig. 2). The bridging ligand X was proposed to be an oxide, hydroxide or hydroperoxide in the oxidized state, and was found to be absent in the reduced state [8–11]. The coordination environment about nickel in the [NiFe] hydrogenases is pseudo-tetrahedral in the reduced state and pseudo-square pyramidal in the oxidized state. Also, the iron site of the [NiFe] hydrogenases isolated from *D. gigas* has been established as a pyramidal $[Fe(CN)_2(CO)]$ unit with the opposite face coordinated to two S-cysteines bridged to a nickel [8–11]. The nickel site has been proposed to be redox active and changes between Ni(III) and Ni(II), while the iron site remains as Fe(II) in all spectrally defined redox states of the enzyme. The active center of [NiFe] hydrogenases exhibits various redox states in the hydrogen catalytic cycle. The EXAFS/EPR studies indicate that the formal oxidation state of the Ni center is paramagnetic Ni(III) in Ni–A, Ni–B and Ni–C states [8–11]. Actually, the active form Ni–C (the paramagnetic Ni–C intermediate) of [NiFe] hydrogenases was proposed to exist as the $[(S_{cys}\text{–}H)Ni^{(III)}\text{–}H\text{–}Fe]$ intermediates after an active state Ni–SIa (silent-active $[(S_{cys}\text{–}H)Ni^{(II)}(S_{cys})_3]$) is passed [8–11]. Ni–R/Ni–SIa states were proposed to exist as $[(S_{cys}\text{–}H)(S_{cys})Ni^{(II)}(\mu\text{-}S_{cys})_2Fe(CO)(CN)_2]$ with a Cys–SH interacting directly with the nickel center (a $[Ni\cdots H\text{–}S_{cys}]$ interaction). In particular, the recent X-ray absorption spectroscopy shows that the Ni site of the regulatory hydrogenase (RH) in the presence of hydrogen (RH^{+H_2}), proposed as Ni–C state, isolated from *Ralstonia eutropha* is a six-coordinated $[Ni^{III}\text{–}S_2(O/N)_3(H)]$ [12].

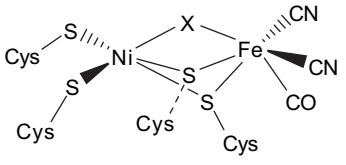

Fig. 2. Schematic drawing of the active site of [NiFe] hydrogenases as deduced from crystallographic studies [8–10].

2. Iron–thiolate complexes with mixed CO/CN^- ligands

2.1. Mimicking the iron part of [NiFe]/[Fe] hydrogenases

Applications of anionic iron(0)–cyanocarbonyl $[Fe(CO)_4(CN)]^-$ for preparation of iron(II)–thiolate cyanocarbonyl proved a successful approach in the synthesis of iron–thiolate cyanocarbonyls. When di(2-aminophenyl) disulfide was reacted with the equal molar $[PPN][Fe(CO)_4(CN)]$ in THF at room temperature, the air-stable, pentacoordinated, 16-electron Fe(II) complex $[PPN][Fe(CO)_2(CN)(S,NH\text{–}C_6H_4)]$ (**1**) was isolated via oxidative addition of disulfide to the $[Fe(CO)_4(CN)]$ motif and subsequent oxygen oxidation accompanied by the concomitant deprotonation of the amine proton (Scheme 1a) [13–15]. The IR spectrum of complex **1** in CH_3CN reveals a weak absorption band for the CN^- ligand at 2099 cm^{-1} while the two strong absorption bands (1997 s, 1933 s cm^{-1}) are assigned to the carbonyl stretching frequencies. When a THF solution of complex **1** is purged with ^{13}CO, the IR ν_{CO} peaks at 1992 and 1928 cm^{-1} immediately shift to 1946 and 1885 cm^{-1} while the IR ν_{CN} stretching frequency remains unchanged. The magnitude $\sim$45 cm^{-1} of the isotopic shift ($\Delta\nu_{CO}$) is consistent with the calculated position, based only on the difference in masses between ^{12}CO and ^{13}CO. The shorter Fe–S bond length of 2.226(2) Å and Fe–N bond length of 1.855(4) Å were attributed to the strong π-donating ability of the bidentate $[S,NH\text{–}C_6H_4]^{2-}$ ligand which stabilized the unsaturated Fe(II) complex **1**.

The dinuclear Fe(II)–thiolate cyanocarbonyl complex $[PPN]_2[(CN)(CO)_2Fe(\mu\text{-}S,S\text{–}C_6H_4)]_2$ (**2**) was prepared in a one-step synthesis by treating 1,2-benzenedithiol with complex **1** in THF under N_2 atmosphere at −10 °C (Scheme 1b). Complex **2** was isolated as an air-stable brown solid at −10 °C. The dinuclear $[(CN)(CO)_2Fe(\mu\text{-}S,S\text{–}C_6H_4)]_2^{2-}$ is electronically dianionic and therefore both irons should be divalent. Each iron atom is surrounded pseudo-octahedrally by two bridging thiolates, one terminal thiolate, two terminal carbonyl groups, and one cyanide ligand. The $Fe^{(II)}\cdots Fe^{(II)}$ distance of 3.472 Å in complex **2** is longer than those reported for the diiron subcluster active site (2.6 and 2.62 Å) of [Fe] hydrogenases [3,4]. The IR spectrum of complex **2** in CH_2Cl_2 reveals a weak absorption band for the CN^- ligands at 2100 cm^{-1}, and two strong absorption bands for the CO groups at 1960 and 2013 cm^{-1} [14–16]. When the CH_2Cl_2 solution of complex **2** was exposed to ^{13}CO at 0 °C, stretching bands $\nu(^{13}CO)$ at

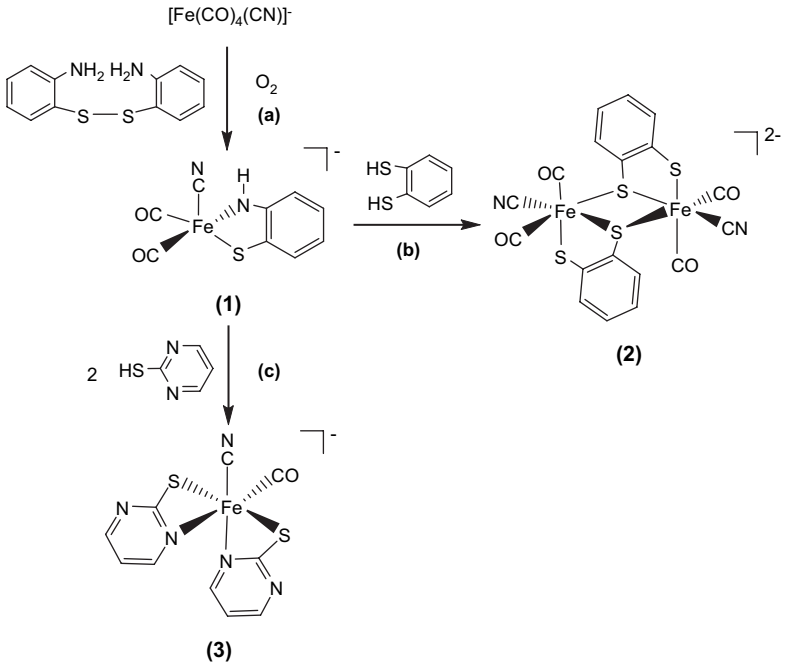

Scheme 1.

1968 and 1915 cm^{-1} appeared within 10 min. Reappearance of the 2013 and 1960 cm^{-1} bands on removal of the ^{13}CO and replacement with ^{12}CO atmosphere demonstrated reversibility of CO ligand lability of complex **2**.

In contrast, protonation of complex **1** by 2 equiv of 2-mercaptopyrimidine in THF under N_2 at ambient temperature yielded hexacoordinated iron(II)–thiolate cyanocarbonyl complex [PPN][Fe(CO)(CN)(S–$C_4H_3N_2$)$_2$] (**3**) with two anionic [S–$C_4H_3N_2$]$^-$ ligands bound to the Fe(II) ion in a bidentate manner (S,N-bound) (Scheme 1c). The IR spectrum of complex **3** in CH_3CN displayed a weak ν_{CN} band at 2090 cm^{-1} and a broad strong ν_{CO} band at 1945 cm^{-1}, well within the range observed for [Fe] hydrogenase isolated from *D. vulgaris* [5]. The reversibility of the CO ligand lability of complex **3** was demonstrated by exposing the CH_2Cl_2 solution of complex **3** to ^{13}CO. The IR ν_{CO} peak at 1948 cm^{-1} shifted to a single absorbance at 1904 cm^{-1} [14]. The vibrational spectroscopies of the $Fe(CO)_2(CN)$ and Fe(CO)(CN) fragments (ν_{CN} ranges from 2087 to 2106 cm^{-1}, ν_{CO} ranges from 1928 to 2013 cm^{-1}) found in complexes **1**–**3** may be regarded as spectroscopic references of [Fe] hydrogenases in the various enzymatic states (Table 1).

Upon cyanogen bromide reacted with [$Fe(CO)_4$(CN)]$^-$ [13] in THF at room temperature, air-stable hexacoordinated Fe(II) complex [PPN][$(CN)_2(CO)_3$Fe(Br)] (**4**) was isolated (Scheme 2a). Subsequent reactions of complex **4** with [Na][S–C(S)–R] (R = OEt, $N(Et)_2$) in THF/CH_2Cl_2 produced the air and thermally stable, yellow *trans*,*cis*-[PPN][$(CN)_2(CO)_2$Fe(S,S–C–R)] complexes (R = OEt (**5**), $N(Et)_2$ (**6**)) individually (Scheme 2b) [17]. The IR ν_{CO}/ν_{CN} data of complexes **4**–**6** are shown in Table 2 [17]. Upon photolysis of THF solution of complex **5** (or **6**) at room

Table 1
Selected infrared data for complexes **1**–**3** and hydrogenases

Compounds	ν_{CN}, cm^{-1}	ν_{CO}, cm^{-1}	Ref.
1	(CH_3CN) 2099	1997, 1933	[14]
	(THF) 2101	1992, 1928	
	(CH_2Cl_2) 2095	2000, 1936	
2	(CH_3CN) 2102	2011, 1961	[14]
	(THF) 2106	2008, 1950	
	(CH_2Cl_2) 2100	2013, 1960	
3	(CH_3CN) 2090	1945	[14]
	(THF) 2094	1942	
	(CH_2Cl_2) 2087	1948	
D. vulgaris, [Fe] hydrogenase	(Air) 2106, 2087	2007.5, 1983, 1847.5	[5a]
	(H_2/Ar) 2095, 2079	2016, 1972, 1965, 1940	
	(H_2/CO) 2096, 2088	2016, 1971, 1964	
	(H_2) 2079, 2041	1965, 1941, 1916, 1894	
Chromatium. vinosum, [NiFe] hydrogenase	2093, 2083	1945	[1c]

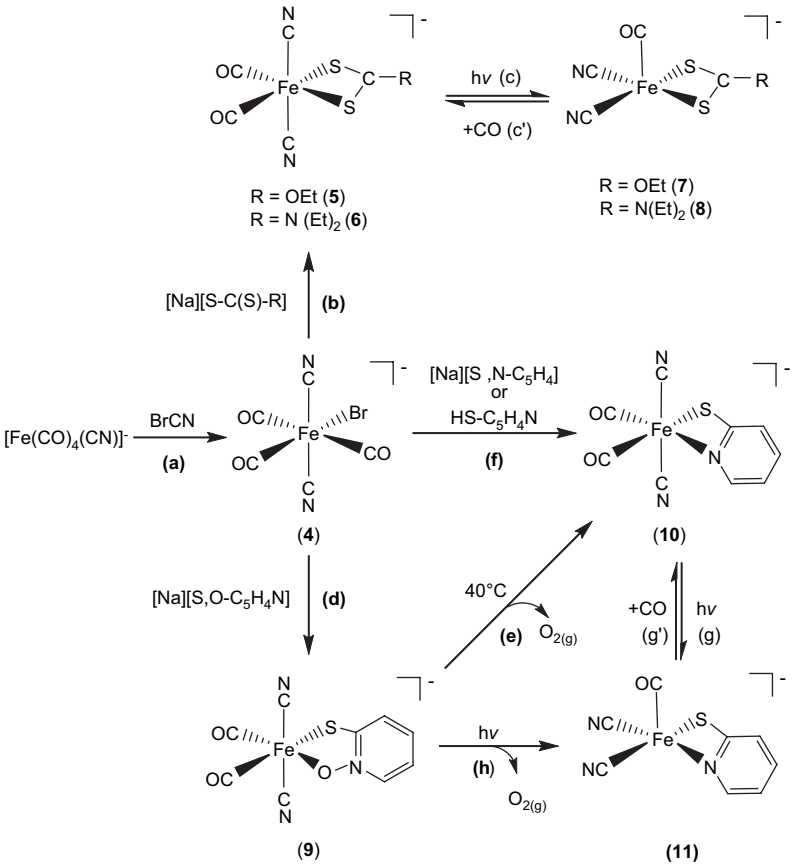

Scheme 2.

temperature, the IR ν_{CO} and ν_{CN} stretching frequencies appeared is consistent with the formation of the coordinatively unsaturated [PPN][$(CN)_2(CO)$Fe(S,S−COEt)] (**7**) ([$(CN)_2(CO)$Fe(S,S−CN$(Et)_2$)]$^-$ (**8**)) (Table 2) with two cyanide ligands occupying *cis* positions (Scheme 2c) [17]. On the basis of density functional theory (DFT) calculation [17], it was found that the square pyramidal complexes **7** and **8** having vacant sites *trans* to the CO ligand are relatively stable [17]. The anionic complexes **7**, **8** and Ni−A/Ni−C states in [NiFe] hydrogenase from *D. gigas* exhibit a similar one-band pattern in the ν_{CO} region and two-band pattern in the ν_{CN} region individually [17,18], but at different positions, 1996 vs (ν_{CO}), 2113 w, 2105 w (ν_{CN}) cm^{-1} (THF) for complex **7**, 1985 vs (ν_{CO}), 2109 w, 2102 w (ν_{CN}) for complex **8** (Table 2), and 1947 vs (ν_{CO}), 2093 w, 2083 w (ν_{CN}) cm^{-1} for Ni−A state [NiFe] hydrogenases isolated from *D. gigas*, which may be accounted for by the distinct electronic effects between [S,S−C−R]$^-$ and cysteine ligands [18]. Also, this result is consistent with the conclusion, reported by Darensbourg et al., that the CO vibrational frequency to the electron density changes around Fe(II) center is about 2.6 times more sensitive than that for CN$^-$ [18c].

In a similar fashion, when a THF solution of complex **4** was treated with 1 equiv of [Na][S,O−C_5H_4N], the d^6 Fe(II) *trans*,*cis*-[PPN][$(CN)_2(CO)_2$Fe(S,O−C_5H_4N)] (**9**) with a five-membered ring (bidentate, S,O-bound) was isolated (Scheme 2d). Subsequently, the four-membered ring *trans*,*cis*-[PPN][$(CN)_2(CO)_2$Fe(S,N−C_5H_4)] (**10**) (bidentate, S,N-bound) along with the presumed O_2 (g)

Table 2
Selected infrared data for complexes **4**–**11** [17]

Compounds	ν_{CN}, cm^{-1} (THF)	ν_{CO}, cm^{-1} (THF)
4	2139 vw, 2127vw	2099 m, 2056s, 2035 m
5	2122 vw, 2112 w	2038 vs, 1984vs
6	2119 vw, 2112 w	2027 vs, 1973 vs
7	2113 w, 2105 w	1996 vs
8	2109 w, 2102 w	1985 vs
9	2121 vw, 2109 w	2041 vs, 1982 vs
10	2124 vw, 2113 w	2036 vs, 1983 vs
11	2111 w, 2103 w	1996 vs

was obtained via thermolytic conversion of complex **9** on heating (40 °C) in THF (Scheme 2e). The S,N-bound complex **10** was alternatively obtained via ligand-substitution reaction, a straightforward reaction of complex **4** with 1 equiv of [Na][S,N–C_5H_4] (or HS–C_5H_4N) in THF (Scheme 2f). To further add credibility to the CO ligand reversibly bound to the Fe^{II} site in these model compounds, a straightforward photolysis of THF solution of complex **10** was also conducted at room temperature, formation of five-coordinated [$(CN)_2(CO)Fe(S,N–C_5H_4)]^-$ (**11**) complex with two cyanide ligands occupying *cis* positions was observed (Scheme 2g). Obviously, photolysis of THF solutions of complexes **5**, **6**, and **10** at room temperature led to the formation of coordinatively unsaturated iron(II)–thiolate dicyanocarbonyl complexes **7**, **8**, and **11**, respectively, with two cyanides occupying *cis* positions and a vacant site preference *trans* to the CO ligand [17]. Additionally, density functional theory (DFT) calculations also suggest the architecture of five-coordinated complexes **7**, **8**, and **11** with a vacant site *trans* to the CO ligand and two CN^- ligands occupying *cis* positions serves as a conformational preference [17]. Presumably, the strong σ-donor, weak π-acceptor CN^- ligands play a major role in creating and stabilizing a five-coordinate iron(II) center with a vacant coordination site [17–19]. The reversibility of CO ligand binding demonstrates that complexes **5/7**, **6/8**, and **10/11** are photochemically interconvertible. This result may implicate the involvement of iron site in the mechanism of hydrogen activation, and can be useful in exploring the key step in H_2 uptake mechanism in [NiFe] hydrogenases. The vibrational spectra of the $[Fe^{(II)}(CN)_2(CO)]$ and $[Fe^{(II)}(CN)_2(CO)_2]$ units (ν_{CO} and ν_{CN}) found in complexes **5–8** may be regarded as spectroscopic references for a variety of [NiFe] hydrogenase enzymatic states, and the exogenously added CO inhibited state, respectively [8–12].

Scrutiny of the coordination chemistry of iron(II)–thiolate cyanocarbonyls $[Fe^{(II)}(CO)_x(CN)_y(SR)_z]^{n-}$ reveals that certain combinations of thiolates and cyanide ligands ($3 \le y + z \le 4$) bound to Fe(II) play an important role in stabilizing the $[Fe^{(II)}(CO)_x(CN)_y(SR)_z]^{n-}$ species [14,17,19], as summarized in Table 3, and this could point the way to understand the reasons for Nature's choice of combinations of these ligands in hydrogenases.

Table 3
Certain combinations of thiolates and cyanide ligands ($3 \le y + z \le 4$) bound to Fe(II) of $[Fe^{II}(CO)_x(CN)_y(SR)_z]^{n-}$ complexes

Compounds	y + Thiolate	Ref.
5	2 + Bidentate	[17]
6	2 + Bidentate	[17]
7	2 + Bidentate	[17]
8	2 + Bidentate	[17]
$[Fe(CO)_2(CN)(CS_3\text{-}S,S)]^-$	1 + Bidentate	[19a]
$[Fe(CO)_2(CN)(S(CH_2)_2S(CH_2)_2\text{-}S\text{-}S,S,S)]^-$	1 + Tridentate	[19a]
$[Fe(CO)_2(CN)_3(SC_6H_4Br)]^{2-}$	3 + Monodentate	[19a]
$[Fe(CO)_2(CN)_2(SPh)_2]^{2-}$	2 + 2(Monodentate)	[19b]
$[Fe(CO)(CN)_2(S_2C_6H_4\text{-}S,S)]^{2-}$	2 + Bidentate	[19b]
$[Fe(CO)_2(CN)_2(S_2C_6H_4\text{-}S,S)]^{2-}$	2 + Bidentate	[19b]

2.2. Dinuclear iron(II)–cyanocarbonyl complexes with bridging ethylthiolates

When complex **4** was reacted directly with [Na][SEt] in THF at room temperature, dinuclear d^6 $Fe^{(II)}$ complex $[PPN]_2[Fe(CN)_2(CO)_2(\mu\text{-}SEt)]_2$ (**12**) was isolated. Attempts to detect the extremely unstable intermediate, the mononuclear $[Fe(CN)_2(CO)_3(SEt)]^-$, by FTIR were unsuccessful (Scheme 3a and b). The $Fe^{(II)}$–$Fe^{(II)}$ distance of 3.505 Å in complex **12** is considerably longer than those reported for the dinuclear iron subcluster (2.6 and 2.62 Å) of the [Fe] hydrogenase active site [3,4]. Here the lack of the third bridging CO ligand and the nearly square planar FeS_2Fe core in complex **12**, in contrast to butterfly structure of the active-site FeS_2Fe core observed in [Fe] hydrogenases, are adopted to rationalize the significantly longer $Fe^{(II)}$–$Fe^{(II)}$ distance in complex **12**. The dinuclear $[Fe(CN)_2(CO)_2(\mu\text{-}SEt)]_2^{2-}$ is electronically dianionic, and therefore both irons should be divalent. Subsequent reactions of complex **12** with [PPN][SEt] in a 1:1 molar ratio in THF produced the thermally stable $[PPN][Fe_2(CN)_2(CO)_4(\mu\text{-}SEt)_3]$ (**13**), and the known *trans*-$[PPN]_2[Fe(CN)_4(CO)_2]$ as identified by IR and X-ray diffraction (Scheme 3c) [6c,20,21].

The $Fe^{(II)}$–$Fe^{(II)}$ distance decreases from 3.505 Å (complex **12**) to 3.073 Å (complex **13**). The considerably longer $Fe^{(II)}$–$Fe^{(II)}$ distance of 3.073 Å in complex **13**, compared to the reported Fe–Fe distances of 2.6/2.62 Å in [Fe] hydrogenases isolated from Dd and Cp [3,4], can be attributed to the presence of the third bridging ethylthiolate, instead of π-accepting CO-bridging ligand as observed in [Fe] hydrogenases. Also, it is noticed that the Fe(II)–Fe(II) distances of complexes $[Fe_2(S_2C_2H_4)(\mu\text{-}CO)(CN)_2(CO)_2(PPh_3)_2]$ containing bridging CO [6c], and $[Fe_2(S_2C_2H_4)(\mu\text{-}H)(CO)_2(PMe_3)_4]^+$ containing bridging hydride [20c] were comparable to 2.6 Å, the reported Fe–Fe distances of [Fe] hydrogenases isolated from Dd and Cp [3,4]. The comparisons of Fe–Fe distances of the reported dinuclear iron–thiolate complexes are collected in Table 4 [3,6c,20].

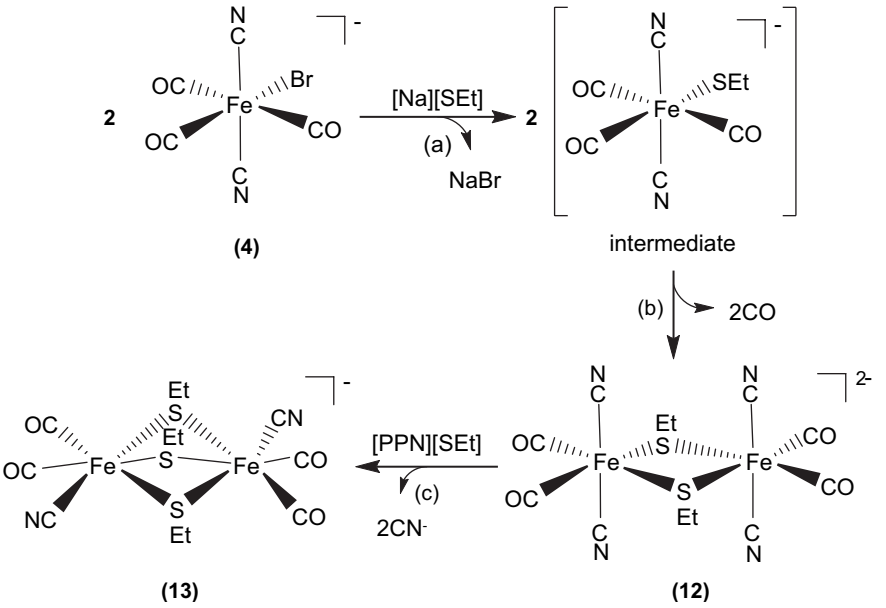

Scheme 3.

3. Nickel–thiolate complexes

3.1. Heterobimetallic nickel–iron complexes

Interesting challenges are in biomimicry of the $[(S_{Cys})_2Ni(\mu\text{-}S_{Cys})_2Fe(CN)_2(CO)]$ active site of [NiFe] hydrogenase. Reaction of the $[Fe(NO)_2(SePh)_2]^-$ (**14**) anion with dimeric $[Ni(\mu\text{-}SCH_2CH_2SCH_2CH_2S)]_2$ in the presence of additional NO_2^- produced the neutral heterobimetallic $[(ON)Ni\{(\mu\text{-}SCH_2CH_2)_2S\}Fe(NO)_2]$ (**15**) (Scheme 4) [22]. According to the Feltham–Enemark notation [23], the distorted tetrahedral iron dinitrosyl group of complex **15** was assigned as $\{Fe(NO)_2\}^9$. The IR ν_{NO} stretching frequencies of complex **15** displayed at 1805, 1767 and 1725 cm^{-1} (CH_2Cl_2) (1798, 1763 and 1723 cm^{-1} in THF) are consistent with an assignment for $\{Ni(NO)\}^9$ $Ni^0(NO)^+$ as is known for analogous phosphine derivatives, $P_3Ni^0(NO)^+$ [24]. The Ni–Fe distance of 2.8 Å in complex **15** is comparable to the natural heterobimetallic Ni–Fe active site found in the [NiFe] hydrogenase enzyme having a Ni–Fe distance of 2.9 Å.

Table 4
The selected dinuclear iron–thiolate complexes

Compounds	Fe–Fe (Å)	ν_{CO}; $\nu_{\mu\text{-}CO}$ (cm^{-1})	Ref.
D. desulfuricans [Fe] hydrogenase	2.6	2016, 1972, 1963, 1811	[3]
12	3.505	2029, 1981 (THF)	[20a]
13	3.073	2029, 2014, 1968 (THF)	[20a]
$Fe_2(S_2C_2H_4)(\mu\text{-}CO)(CN)_2(CO)_2(PPh_3)_2$	2.546	2004, 1993; 1904 (μ-CO)	[6c]
$[Fe_2(S_2C_2H_4)(\mu\text{-}H)(CO)_2(PMe_3)_4]^+$	2.610	1940, 1928 (CH_3CN)	[20b]
$[Fe_2(S_2C_2H_4)(\mu\text{-}CO)(H)(CO)(PMe_3)_4]^+(\mu\text{-}CO)$	2.566	1940; 1874 (CH_3CN)	[20b]
$[Fe_2(MeSCH_2C(Me)(CH_2S)_2)(CN)_2(CO)_3(\mu\text{-}CO)]^-$		1945, 1978, 2030; 1790 (μ-CO)	[20c,d]
$[Fe_2(MeSCH_2C(Me)(CH_2S)_2)(CN)_2(CO)_3(\mu\text{-}CO)]^{2-}$		1878, 1919, 1957; 1780 (μ-CO)	[20c,d]

In particular, complex $[Fe(CO)_2(CN)_2(\mu\text{-pdt})Ni(S_2CNEt_2)]^-$ with bridging 1,3-propanedithiolate ligand and iron center coordinated by two CO and two CN^-, the precise model of the active site of the reduced-form [NiFe] hydrogenase, was isolated and characterized by IR and single-crystal X-ray structure [22f]. The selected heterodinuclear Ni–Fe–thiolate complexes are collected in Table 5.

3.2. Mononuclear nickel(II) carbonyl complexes

A THF mixture solution of $[CpNi(CO)]_2$ and $(PhSe)_2$ added to the acetonitrile (THF) solution of *fac*-$[PPN][Fe(CO)_3(SePh)_3]$ (1:1:2 molar ratio) yielded $[PPN][Ni(CO)(SePh)_3]$ (**16**) and byproduct $[CpFe(CO)_2(SePh)]$ [25,26]. The sequences of reactions given in Scheme 5 rationalizes the formation of complex **16** and $[CpFe(CO)_2(SePh)]$. The oxidative addition of

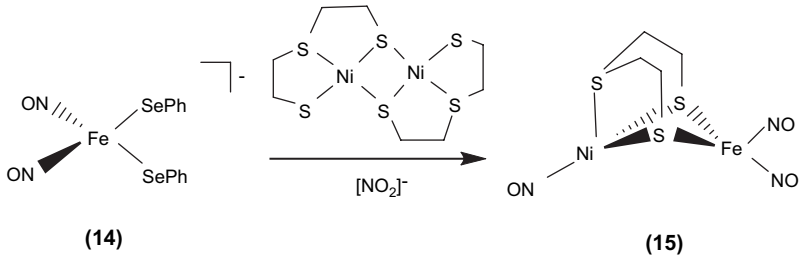

Scheme 4.

diphenyldiselenide across the Ni–Ni bond of $[CpNi(CO)]_2$, and nucleophilic attack of an incoming tridentate motif *fac*-$[Fe(CO)_3(SePh)_3]^-$ resulting in the bridged-selenolate cleavage was presumed to be accompanied by cyclopentadienyl $[C_5H_5]^-$ ligand-transfer from Ni(II) to Fe(II), the concomitant Fe(II)–SePh bond cleavage, and a labile carbonyl ligand shifting from Fe(II) to Ni(II) led to the formation of $[Ni(CO)(SePh)_3]^-$ and $CpFe(CO)_2(SePh)$ [26]. Compared to the ν_{CO} band of pentacoordinated Ni(I)/Ni(II) carbonyl complexes $[Ni(NS_3{}^tBu)(CO)]^+$ (2026 cm^{-1}) [27], $[Ni(DAPA)(SePh)_2(CO)]^-$ (2024 cm^{-1}) [28], and $[Ni(PS3^*)(CO)]^-$ (2029 cm^{-1}) [29], complex **16** displays a IR ν_{CO} band at 2023 cm^{-1}. When a THF solution of $[Ni^{(II)}(CO)(SePh)_3]^-$ was purged with ^{13}CO, the IR ν_{CO} peak at 2023 cm^{-1} immediately shifts to a single absorbance at 1976 cm^{-1}. Reaction of complex **16** with 1 equiv of $(PhS)_2$ in THF results in the formation of the extremely air-sensitive $[Ni(CO)(SPh)(SePh)_2]^-$ (compared to $[Ni(CO)(SePh)_3]^-$). In a similar fashion, $[Ni(CO)(SePh)_3]^-$ was reacted with $(PhS)_2$ in a 1:2 molar ratio to yield $[Ni(CO)(SPh)_2(SePh)]^-$ [30].

Table 5
The selected heterodinuclear Ni–Fe–thiolate complexes

Compounds	Ni/Fe valence	Ni–Fe distance (Å)	Ref.
D. gigas$_{ox}$	3+, 2+	2.9	[1a,1b]
15	0, 1+	2.8	[22a]
[{Fe('S_3')(CO)(PMe_3)$_2$-S,S′} Ni('S_2')][a]	2+, 2+	3.32	[22b]
$[Ni(L)Fe(CO)_4]$[b]	0, 2+	3.76	[22c]
[{$Ni(SCH_2CH_2CH_2S)$(dppe)-S,S′} $Fe(CO)_3$][c]	0, 2+	2.47	[22d]
[{$Fe(NS_3)(CO)_2$-S,S′}NiCl(dppe)][d]	2+, 2+	3.31	[22e]
$[Fe(CO)_2(CN)_2(\mu\text{-pdt})Ni(S_2CNEt_2)]^-$[e]	2+, 2+	2.9	[22f]
$[(dppe)Ni(pdt)Fe(Cp)(CO)]^+$		2.78	[22g]

[a] 'S_3'$^{2-}$ = bis(2-mercaptophenyl)sulfide(2−); 'S_2'$^{2-}$ = 1,2-benzenedithiolate.
[b] L = *N*,*N*′-bis(2-mercaptoethyl)-1,5-diaza-cyclooctane.
[c] dppe = 1,2-bis(diphenyl-phosphino)ethane.
[d] NS_3 = $N(CH_2CH_2S)_3^{3-}$.
[e] pdt = 1,3-propanedithiolate.

3.3. Mononuclear nickel(II)–thiolate complexes with pendant thiol

Study on the structures and reactivity of Ni(II)–thiol and Ni(III)–thiolate complexes may be useful in interpreting the catalytic cycle of H_2 activation in [NiFe] hydrogenase. In model compounds, an electrochemical study provided evidence of formation of a Ni(III)–H species generated by one-electron reduction of a nickel(II) macrocyclic complex accompanied by protonation [31]. Reaction of complex **16** with tris(2-phenylthiol)-phosphine ($P(o\text{-}C_6H_4SH)_3$) produced the four-coordinated [PPN][Ni(SePh)($P(o\text{-}C_6H_4S)_2(o\text{-}C_6H_4SH)$)] (**17**) [32]. Complex **17** containing pendant thiol stabilized by an intramolecular S–H proton directly interacting

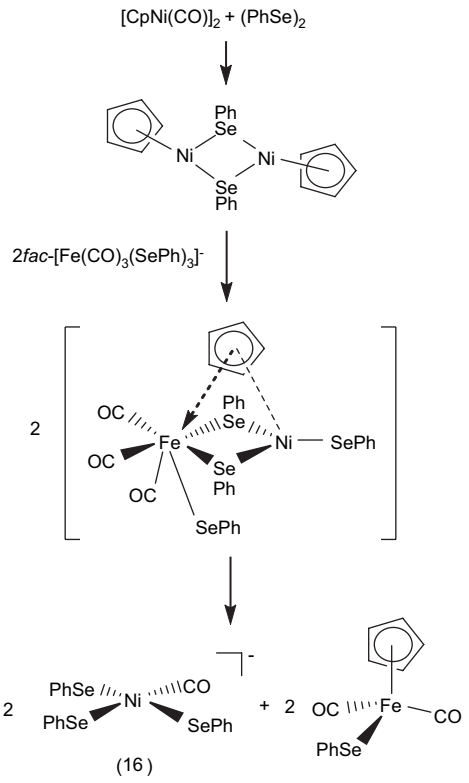

Scheme 5.

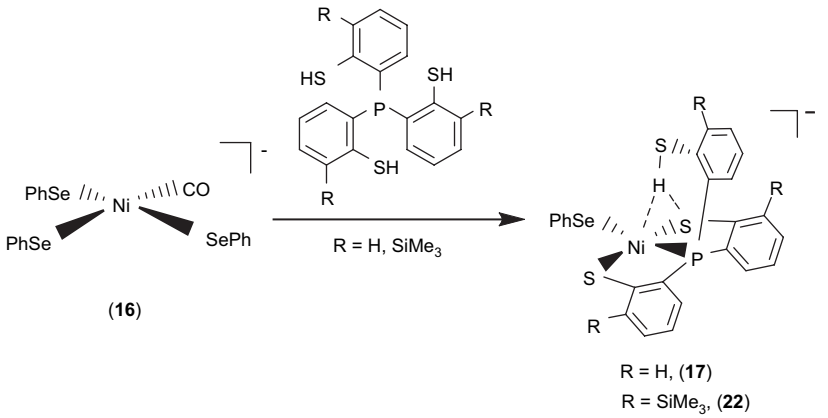

Scheme 6.

with both nickel and sulfur atoms was synthesized and characterized by IR, ^{1}H NMR, UV–vis, and X-ray diffraction (Scheme 6). The infrared KBr solid spectrum of complex **17** shows one broad stretching band (2273 cm^{-1}) in the ν_{S-H} region. The lower energy ν_{S-H} band of complex **17** shifted by ~215 cm^{-1} from that of the free ligand P(*o*-$C_6H_4SH)_3$ (2488 cm^{-1}) implies the specific [Ni–S···H–S]/[Ni···H–S] interactions [32,33]. Intramolecular [Ni–S···H–S]/[Ni···H–S] interactions in complex **17** also result in the ^{1}H NMR chemical shift of the SH group, shifting from δ 4.07 (d) ppm ($CDCl_3$) in free ligand P(*o*-$C_6H_4SH)_3$ to δ 8.079 (d) ppm (S–H) (CD_2Cl_2) in complex **17** [32,33]. The intramolecular interaction is best interpreted in terms of the thiol proton interacting with both sulfur and nickel atoms, where the proton is bound to sulfur and ''attracted'' by the Ni(II) and the second sulfur atom, that is, a combination of [Ni–S···H–S]/[Ni···H–S] interactions. The H/D exchange reaction between complex **17** and D_2O occurred in CH_3CN–THF solution (1:3 volume ratio) at 5 °C as indicated by IR and ^{2}H NMR. The IR ν_{S-H} at 2273 br cm^{-1} shifting to absorbance at 1676 br cm^{-1} (ν_{S-D}, KBr) is roughly consistent with the calculated position, based only on the difference in masses between S–H and S–D. The interactions [Ni–S···H–S]/[Ni···H–S] may contribute to the stabilization of Ni(II)–thiol complex **17**.

A comparison of IR ν_{S-H} and ^{1}H NMR data of analogues [PPN][Ni(X)(P(*o*-$C_6H_4S)_2$(*o*-C_6H_4SH))] (X = PPh_3 (**18**), S–C_4H_3S (**19**), Cl (**20**), Se–*p*-C_6H_4–Cl (**21**)) and $SiMe_3$-substituted complexes [PPN][Ni(X)(P(*o*-C_6H_3–3-$SiMe_3$–2-$S)_2$(*o*-C_6H_3–3-$SiMe_3$–2-SH))] (X = SePh (**22**), Cl (**23**)) with intramolecular [Ni–S···H–S]/[Ni···H–S] interactions is provided in Table 6 (Scheme 6) [32,34–36]. These results show that electronic modulations of the monodentate ligand of complexes **17**–**23** are capable of inducing different degree of interacting strength of the intramolecular [Ni–S···H–S] and [Ni···H–S] interactions.

Alternatively, reaction of $NiCl_2(PPh_3)_2$ and tris(2-phenylthiol)phosphine (P(*o*-$C_6H_4SH)_3$) in THF also led to the isolation of the red-brown four-coordinated Ni(II) [Ni(PPh_3)(P(*o*-$C_6H_4S)_2$(*o*-C_6H_4SH))] (**18**) (Scheme 7) [35]. When a THF solution of complex **18** was recrystallized with THF–hexane, complex **18a** displaying a broad ν_{S-H} stretching band at 2393 cm^{-1} (KBr) was isolated and characterized by X-ray crystallography (Scheme 7). In contrast, the diffusion of hexane into a CH_2Cl_2 solution of complex **18** yielded complex **18b** with a broad ν_{S-H} stretching band at 2240 cm^{-1} (KBr), characterized by single-crystal diffraction (Scheme 7). The IR spectra of complexes **18a** and **18b** display broad ν_{S-H} stretching bands at 2393 and 2240 cm^{-1} (KBr), which are ~90 and ~250 cm^{-1} lower than the free ligand 2488 cm^{-1}

Table 6
Selected infrared and ^{1}H NMR data for complexes **17**–**23** and **35**

Compounds	ν_{S-H}, cm^{-1} (KBr)	^{1}H NMR, δ	Ref.
P(*o*-$C_6H_4SH)_3$	2488	4.07 (d) ($CDCl_3$)	[33]
P(C_6H_3–3-$SiMe_3$–2-$SH)_3$	2466	4.58 (br) ($CDCl_3$)	[33]
17	2273	8.079 (d) (CD_2Cl_2)	[32]
18a	2393	5.908 (s) ($CDCl_3$)	[35]
18b	2240	5.908 (s) ($CDCl_3$)	[35]
19	2283	8.39 (d) (C_4D_8O)	[32]
20	2300	5.808 (s) ($CDCl_3$)	[35]
21	2288	8.39 (d) (C_4D_8O)	[35]
22a	2250	8.59 (br) (C_4D_8O)	[39]
22b	2137	8.59 (br) (C_4D_8O)	[39]
23a	2287	8.54 (br) (C_4D_8O)	[39]
23b	2235	8.54 (br) (C_4D_8O)	[39]
35	2385	6.24 (d) ($CDCl_3$)	[39]

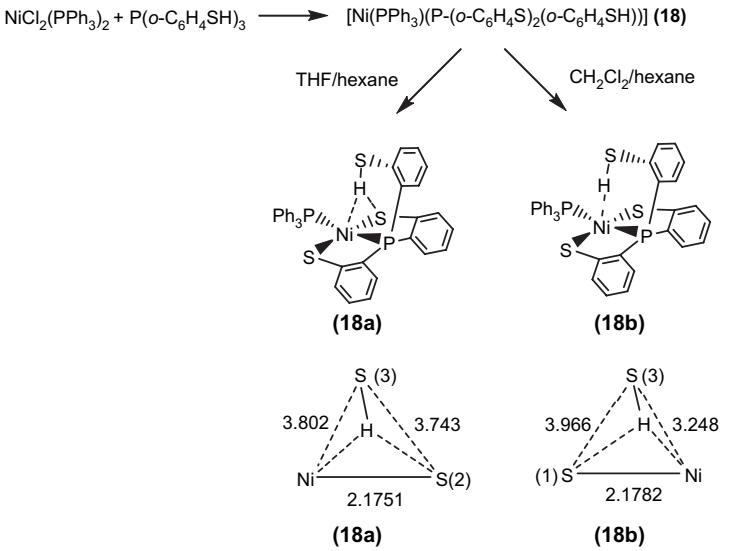

Scheme 7.

(KBr), respectively. This lower ν_{S-H} stretching frequency may imply the existence of intramolecular [Ni–S···H–S]/[Ni···H–S] interactions. In complex **18a**, the acute (C–S–H) bond angle of 95.04° and the similar distances of Ni···S(3) (3.802 Å) and S(2)···S(3) (3.743 Å) suggested that the proton of S(3)–H points toward the middle of the Ni and S(2) atoms, and interacts with both sulfur (S(2)) and nickel atoms (i.e., a combination of the intramolecular [Ni–S···H–S]/[Ni···H–S] interactions, Scheme 7). In contrast, the Ni···S(3) distance of 3.248 Å is significantly shorter than the S(1)···S(3) distance of 3.966 Å in complex **18b**. Compared to complex **18a**, the acute (C–S–H) bond angle of 99.64° and a lower ν_{S-H} stretching band (2240 cm^{-1} (KBr)) in complex **18b** may indicate that the thiol proton tends to interact directly with the nickel atom (i.e., a [Ni···H–S] interaction) (Scheme 7) [35]. Similarly, two forms of crystalline products **22a/23a** (plate-shaped, red-brown crystals) and **22b/23b** (block-shaped, dark-red crystals) were also obtained when **22/23** were recrystallized from THF–diethyl ether and THF–hexane, respectively, at room temperature [36].

Complex **18** serves as a precursor for the syntheses of the anionic mononuclear $Ni^{(II)}$–thiol complexes **19–21** via a ligand-displacement reaction. Addition of $[SePh]^-$ (or $[S-C_4H_3S]^-$, $[Cl]^-$ and $[Se-p-C_6H_4-Cl]^-$) to the CH_3CN–THF solution (1:3 volume ratio) of complex **18** at 0 °C for 4 h afforded the ligand-displacement complex **17** (or **19–21**) identified by IR, NMR, UV–vis and single-crystal X-ray diffraction, respectively, (Scheme 8a and b) [35]. In contrast to the ligand displacemeant occurring in the reaction of complex **18** and the anionic $[SePh]^-$ (or $[Cl]^-$/$[Se-p-C_6H_4-Cl]^-$), addition of $[SR]^-$ (R = Ph, Et) to complex **18** yielded mononuclear $[PPN][Ni^{II}(PPh_3)(P(o\text{-}C_6H_4S)_3)]$ (**24**) by the liberation of thiophenol (or ethanethiol) identified by ^1H NMR spectra (Scheme 8c). Protonation of complex **24** in THF at 0 °C by $HClO_4$ produced complex **18** (Scheme 8c′). Treatment of $[Me_3O][BF_4]$ and complex **24** in a CH_3CN–THF solution (1:3 volume ratio) yielded the $[Ni^{II}(PPh_3)(P(o\text{-}C_6H_4S)_2(o\text{-}C_6H_4-SCH_3))]$ (**25**) identified by single-crystal X-ray diffraction (Scheme 8d) [35]. On the basis of the single-crystal X-ray diffraction, two different conformational isomers of complex **25** were isolated. The green crystals of complex **25a** were obtained by diffusion of hexane into the THF solution of complex **25** at 0 °C. Interestingly, diffusion of hexane into the THF solution of complex **25** at 30 °C produced green crystals (complex **25a**) and red crystals which were identified by single-crystal X-ray diffraction as complex **25b** (Scheme 9). Each crystal form shows identical ^1H NMR spectroscopic properties (methyl (CH_3) proton resonance at 2.021 ppm) ($CDCl_3$)) when complexes **25a** and **25b** were redissolved, respectively, in $CDCl_3$ at room temperature [35]. Obviously, these two conformational isomers (**25a** and **25b**) are in equilibrium via intramolecular rearrangement controlled by the temperature of solution. In contrast to the temperature-dependent interconversion of the conformational isomers **25a** and **25b**, the temperature-independent four-coordinated Ni(II)–thioether complexes $[Ni^{(II)}(L)$

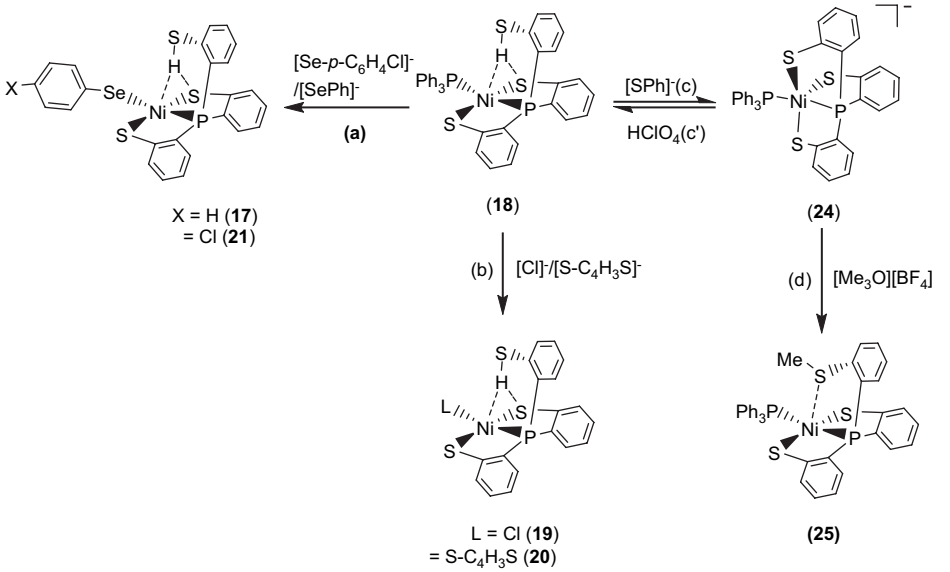

Scheme 8.

$(P(o\text{-}C_6H_4S)_2(o\text{-}C_6H_4{-}SCH_3))]^-$ (L = SPh (**26**), SePh (**27**)) were isolated when complex **25** was reacted with $[SPh]^-$ and $[SePh]^-$, respectively, in THF at room temperature overnight (Scheme 10) [35].

Compared to the Ni···S(3) distances of 3.802 and 3.248 Å observed in complexes **18a** and **18b** (Scheme 7), the single-crystal X-ray structure revealed that thioether sulfur semibonding to Ni(II) (Ni···S(3) distance of 2.5397 Å) may exist in complex **25a** and that there is no interaction between Ni and S(3) (Ni···S(3) distance of 2.9135 Å) in complex **25b** (Scheme 9). Obviously, on the basis of the ^{1}H NMR spectra and single-crystal X-ray diffractions, the intramolecular interaction between Ni^{II} and the thioether sulfur atom became weaker when the temperature was increased or the more electron-donating monodentate ligand was ligated to the $Ni^{(II)}$ center, as observed in the mononuclear $Ni^{(II)}$–thioether complexes **25a**, **25b**, **26** (Ni···S(Me) distance of 3.258 Å), and **27** (Ni···S(Me) distance of 3.229 Å; Scheme 10). Presumably, increasing the electron density surrounding Ni should have the opposite effect on the interaction with RSH and RSR′. Increasing the electron density on Ni favors the interaction with S–H (Ni acts as a hydrogen-bond acceptor) and disfavors the interaction with S in SRS′ (RSR′ is an electron pair donor) [35].

In complexes **17**–**21**, the presence of the intramolecular [Ni–S···H–S] interaction (or a combination of intramolecular [Ni–S···H–S] and [Ni···H–S] interactions) was verified in the solid state by the observation of a lower IR ν_{S-H} stretching frequency compared to that of the free ligand $P(o\text{-}C_6H_4SH)_3$ (Table 6), and was subsequently confirmed by single-crystal X-ray diffraction. As shown in Scheme 11, single-crystal X-ray diffraction studies reveal that the Ni···S(1) distance falls into the range of 3.609–3.802 Å in Ni(II)–thiol complexes **17**, **18a** and **19**–**21** (Scheme 11, type A), compared to those of 2.540 and 2.914 Å in the Ni(II)–thioether complexes **25a** and **25b** (Scheme 11, type C). In contrast, the long Ni···S(1) distances (3.258 and 3.229 Å) found in complexes **26** and **27** indicated the absence of interaction between the Ni and S(1) atoms (Scheme 11, type D). These results rule out the existence of an intramolecular Ni···S(1) interaction (Ni···S(1) distance of 3.609–3.802 Å) in complexes **17**, **18a** and **19**–**21** (Scheme 11, type B) and may support the idea that the pendant thiol proton of complexes **17**–**21** were attracted by both nickel and sulfur of thiolate, resulting in combinations of intramolecular [Ni–S···H–S] and [Ni···H–S] interactions (Scheme 11, type A) [35].

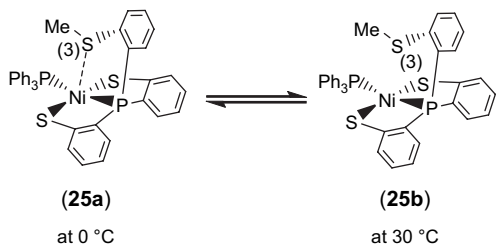

Scheme 9.

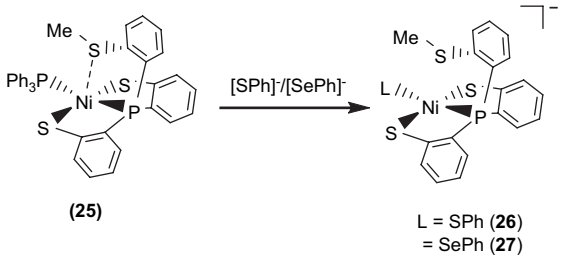

Scheme 10.

3.4. Mononuclear nickel(III)–thiolate complexes

The mononuclear Ni(III) complex [PPN][Ni(SePh)($P(o\text{-}C_6H_4S)_3$)] (**28**) identified by ^{1}H NMR, EPR, UV–vis, SQUID and X-ray diffraction was obtained upon addition of dry O_2 to complex **17** (Scheme 12a). The 4.2 K EPR spectrum of complex **28** exhibits high rhombicities with three principal g values of 2.304, 2.091, and 2.0. There is no ^{31}P hyperfine coupling observed under various conditions, even in ENDOR detection. The average g value ($g_{av} = 2.132$) that is much higher than the spin-only g value 2.0023 indicates large orbital contribution to the paramagnetism, suggesting that the unpaired electron is associated primarily with the nickel ion [32,36]. The ^{1}H NMR spectrum of complex **28** at 298 K shows the expected paramagnetic properties. The effective magnetic moment in the solid state by SQUID magnetometer was 1.91 μ_B for complex **28**, which is consistent with the Ni^{III} having a low-spin d^7 electronic configuration in a distorted trigonal bipyramidal ligand field [32,36]. The 4.2 K EPR signals of complex **28** with three principal g values of 2.304, 2.091, and 2.0 are comparable with the g values near 2.31, 2.24, and 2.01 (for Ni–A) and 2.33, 2.16, and 2.01 (for Ni–B) ascribed to Ni(III) observed in the oxidized Ni–A as well as Ni–B states of [NiFe] hydrogenases, a formal Ni(III) in a $3(d_{z^2})^1$ electronic configuration. The most noteworthy characteristic of complex **28** is the existence of a reversible, metal-based reduction with the $Ni^{(III/II)}$ redox potential $E_{1/2} = -0.67$ V vs Ag/AgCl ($\Delta E_p = 0.07$ V, scan rate = 0.1 V/s) in MeCN, which is comparable to the $Ni^{(III/II)}$ redox potentials, ca. −390 to −640 mV vs SCE of [NiFe] hydrogenases [37]. The stable mononuclear Ni(III)–thiolate complex **28** is soluble in CH_2Cl_2/THF–CH_3CN, and form a thermally sensitive, air-sensitive solution in organic solvents. On the basis of this investigation and related observations, it is presumed that the polarizable anionic thiolate/selenolate donor ligand and a relatively rigid tetradentate ligand in complex **28** place Ni(III) in an optimum electronic condition to minimize the possibility of autoreduction of Ni(III) and to prevent the formation of polynuclear nickel–thiolate species.

In a similar fashion, the mononuclear Ni(III) complex [PPN][Ni(SePh)($P(o\text{-}C_6H_3\text{–}3\text{-}SiMe_3\text{–}2\text{-}S)_3$)] (**29**) was obtained upon addition of dry O_2 to complex **22** [36]. As shown in Scheme 12b, addition of CH_2Cl_2 to complex **29** in the absence of dioxygen produced [PPN][$Ni^{(III)}$(Cl)($P(C_6H_3\text{–}3\text{-}SiMe_3\text{–}2\text{-}S)_3$)] (**30**). In displacement reaction, complexes [PPN][Ni(SR)($P(C_6H_3\text{–}3\text{-}SiMe_3\text{–}2\text{-}S)_3$)] (R = ethyl (**31**), 2-thienyl (**32**)) containing coordinated ethylthiolate (or 2-thienylthiolate) were synthesized by adopting complex **30** serving as a precursor (Scheme 12c). The single-crystal X-ray structure shows a Ni(III)–SEt bond length of 2.273(1) Å in complex **31** is in the range of 2.12–2.28 Å for the Ni(III)–S bond lengths of the oxidized *D. gigas* hydrogenases [8–10]. The EPR spectra of complexes **29**–**31** are identical at 77 K and exhibit rhombicity with principal g values of 2.31, 2.09, and 2.0 [36].

When a THF–CH_3CN (3:1 v/v) solution of complex **29** (or complexes **31** and **32**) was treated with CO (1 atm) at ambient temperature, complex **29** (or complexes **31** and **32**) completely transformed into complex [PPN][Ni(II)(CO)($P(C_6H_3\text{–}3\text{-}SiMe_3\text{–}2\text{-}S)_3$)] (**33**)

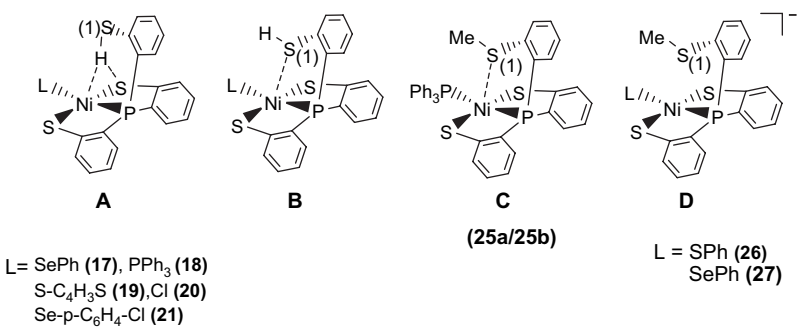

Scheme 11.

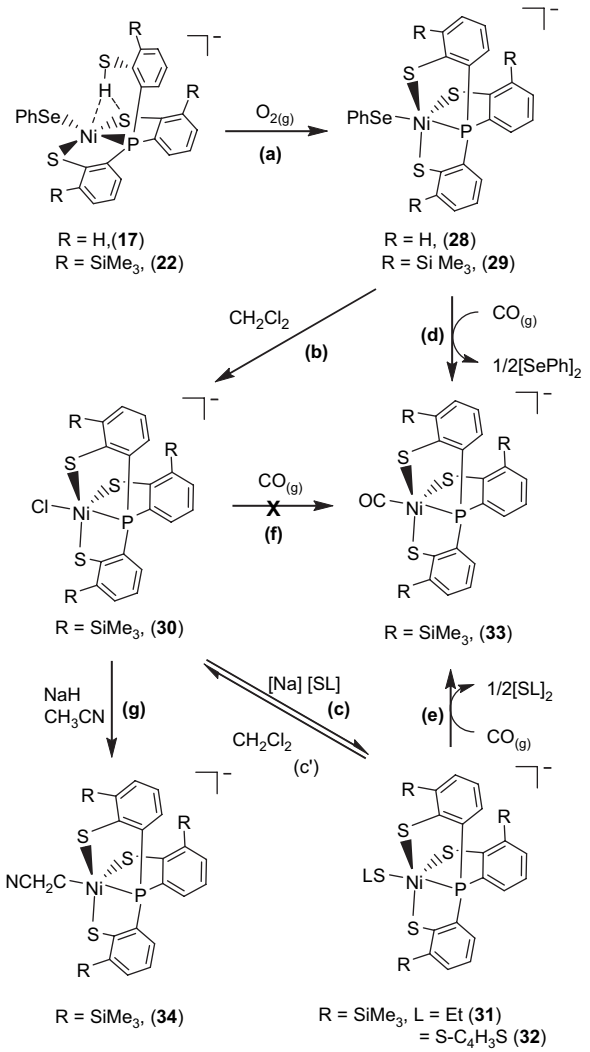

Scheme 12.

accompanied by the formation of diphenyldiselenide (diethyl disulfide, di(2-thienyl) disulfide) identified by ^{1}H NMR spectrum (Scheme 12d and e). Obviously, CO molecule triggers the reductive elimination of the coordinated phenylselenolate of complex **29** (or ethylthiolate of complex **31**, 2-thienylthiolate of complex **32**) to yield Ni(II)–CO complex **33** and byproduct $(PhSe)_2$ (or $(SEt)_2$/$(2\text{-S}-C_4H_3S)_2$), relevant to the observation that Ni–C state was converted into the Ni–L form under illumination, which subsequently transformed into Ni–CO state under exogenous CO condition in [NiFe] hydrogenase isolated from *D. vulgaris* Miyazaki F. [9c,d]. It is presumed that the σ-/π-electron-donating nature of the coordinated thiolates/selenolate converts Ni(III), a weaker π-donor, into a strong π-donor and favors Ni–CO bonding by reductive elimination [26,36,30]. This result implies that the Ni(III)–Cl bond of complex **30** is resistant to undergo reductive elimination, in contrast to the Ni(III)–SePh and Ni(III)–SEt bonds of complexes **29** and **31**, respectively (Scheme 12f). The Ni(II)–CO of complex **33** is not photolabile. THF solution of complex **33** is stable under photolysis ($\lambda = 365$ nm) for 7 h at ambient temperature. The unprecedented nickel(III)–thiolate complex containing C-bonded cyanomethanide [PPN][Ni(CH_2CN)(P(C_6H_3–3-$SiMe_3$–2-S)$_3$)] (**34**) was also isolated from reaction of complex **30** and CH_3CN in the presence of NaH at ambient temperature (Scheme 12g) [36]. Carbon monoxide did not trigger the reductive elimination of Ni(III)–CH_2CN bond, even exposing the CH_3CN solution of complex **34** under 1 atm of CO at ambient temperature for 4 days [38]. In contrast to the inertness of complexes **30** and **34** under a CO atmosphere, carbon monoxide did trigger the reductive elimination of the monodentate chalcogenolate ligand of complexes **29**, **31**, and **32** to yield Ni^{II}–CO complex **33** accompanied by the formation of diphenyl/dialkyl dichalcogenides [36]. This result may provide some clues to the transformation mechanism between the Ni–L form and Ni–CO form of [NiFe] hydrogenase isolated from *D. vulgaris* Miyazaki F. and CO acting as an inhibitor for catalytic activity of [NiFe] hydrogenases [36,37]. It is anticipated that the Ni(III)–alkylthiolate complexes containing an optimum electronic condition around the Ni center may trigger heterolytic H_2 cleavage via the cooperation of Ni(III) and the coordinated $[SR]^-$ ligand.

4. Dinuclear nickel–thiolate complexes

Investigation of the relationship between the core geometry of the bimetallic [Ni–Fe]/[Ni–Ni] center and the oxidation levels of nickel is limited. The neutral dinuclear Ni(II) complex [Ni(P(*o*-C_6H_3–3-$SiMe_3$–2-S)$_2$(*o*-C_6H_3–3-$SiMe_3$–2-SH))]$_2$ (**35**) was prepared by ethylation of [PPN][Ni(SePh)(P(*o*-C_6H_3–3-$SiMe_3$–2-S)$_2$(*o*-C_6H_3–3-$SiMe_3$–2-SH))] (**22**) (Scheme 13a). Complex **35** exhibits extreme air sensitivity in solution (THF, diethyl ether) [39]. Compared to complexes **22a/22b** (IR ν_{S-H} 2250 and 2137 cm^{-1} (KBr)), the higher ν_{S-H} stretching frequency (2385 cm^{-1} (KBr)) of complex **35** implies the absence of intramolecular [Ni–S···H–S] interactions (Table 6). The elongation of two Ni···S–H distances (3.947(1) and 3.868(1) Å, respectively) in **35**, compared to the Ni···S–H distance of 3.690(1) and 3.305(1) Å in **22a** and **22b**, respectively, also implicates the absence of the intramolecular [Ni–S···H–S] interactions. Formation of complex **35** via the coordinative association

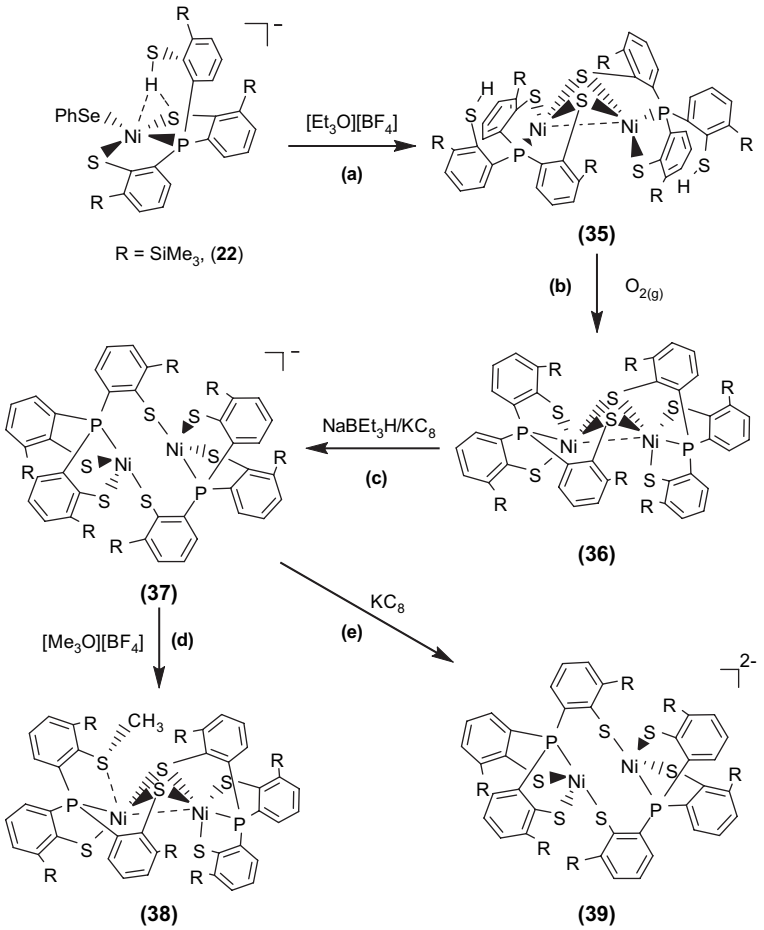

Scheme 13.

of two [Ni(II)P(*o*-C_6H_3–3-$SiMe_3$–2-S)$_2$(*o*-C_6H_3–3-$SiMe_3$–2-SH)] units can lend support to the previous proposal that the distinct electron-donating ability of the coordinated ligands may serve to regulate the intramolecular [Ni–S···H–S]/[Ni···H–S] interactions [35]. The geometry about both of the central Ni(II) can be regarded as slightly distorted square planar and the Ni···Ni distance of 2.5808(8) Å is short enough to suggest a certain degree of interaction between two Ni(II) centers of complex **35** [39]. Oxygen oxidation of complex **35** yielded the thermally stable dinuclear Ni(III) [Ni(III)(P(*o*-C_6H_3–3-$SiMe_3$–2-S)$_2$(*o*-C_6H_3–3-$SiMe_3$–2-μ-S))]$_2$ (**36**) accompanied by the byproduct H_2O identified by ^{1}H NMR (Scheme 13b). Complex **36** in frozen CH_2Cl_2 shows EPR silent at 77 K. On the basis of ^{1}H NMR, EPR, and magnetic measurements, complex **36** was characterized as a diamagnetic species. Thus, the electronic structure of complex **36** can be best described as two paramagnetic d^7 Ni(III) cores with antiferromagnetic coupling ($J = -3.13$ cm^{-1}), that is, both Ni(III) centers have $S = 1/2$ spins magnetically coupled to each other possibly via the direct d–d orbital overlap (Ni···Ni = 2.6026(7) Å) and the bridging sulfurs. Both complexes **35** and **36** show the butterfly structure of the Ni(μ-S)$_2$Ni unit on going from Ni(II) complex **35** to Ni(III) complex **36** with little Ni–S–Ni bond angles and a Ni···Ni distance change (Ni–S–Ni bond angles of 70.59 (4)/70.33 (4)° and a Ni···Ni distance of 2.5808 (8) Å for **35**, and 70.05 (3)/70.18 (3)° and 2.6026 (7) Å for **36**) [39].

The fully delocalized mixed-valence [Ni(II)Ni(III)] complexes [Ni$_2$(P(*o*-C_6H_3–3-$SiMe_3$–2-S)$_3$)$_2$]$^-$ (**37**) and [Ni$_2$(P(*o*-C_6H_3–3-$SiMe_3$–2-S)$_3$)(P(*o*-C_6H_3–3-$SiMe_3$–2-S)$_2$(*o*-C_6H_3–3-$SiMe_3$–2-SCH_3))] (**38**) were isolated upon the reduction of complex **36** and the methylation of complex **37**, respectively (Scheme 13c and d). Compared to the rhombic signal with *g* values of 2.31, 2.09, and 2.0 (77 K) observed in complex **29**,

the 77 K EPR spectrum of complex **37** exhibits high rhombicities with three principal g values of 2.113, 2.073, and 2.033 (an isotropic signal with a g value of 2.077 at 298 K) [39]. The UV–vis spectrum of complex **37** exhibits an intense absorption around 1124 nm with an extinction coefficient $\varepsilon > 2000\ \mathrm{L\,mol^{-1}\,cm^{-1}}$, which may be ascribed to the intervalence transition of the fully delocalized mixed-valence complexes. These results support that complex **37** adopts a fully delocalized mixed-valence [Ni(III)–Ni(II)] electronic configuration in a distorted square planar ligand field. The geometrical rearrangement from the butterfly structure of [Ni(μ-S)$_2$Ni] unit of complex **36** to the diamond shape of [Ni(S)$_2$Ni] core of complex **37** reflects the effects caused by the addition of one electron. Upon one-electron reduction of complex **36** yielding complex **37**, the Ni···Ni distance is lengthened by as much as 0.22 Å. The apparently shorter Ni···Ni distance (2.6088(11) Å) of complex **36**, compared to the Ni···Ni distance of 2.829(1) Å in complex **37**, indicates a greater extent of Ni···Ni interaction in complex **36**. The electronic perturbation caused by the sulfur methylation of complex **37** triggers the stronger Ni···Ni interaction accompanied by the geometrical rearrangement from the diamond shape of the [Ni(S)$_2$Ni] core of complex **37** to the butterfly structure of the [Ni(μ-S)$_2$Ni] unit of complex **38** to reimburse the deficiency of electron density surrounding [Ni(II)-Ni(III)] centers. Interestingly, the frozen-solution EPR spectrum of complex **38** (77 K) in diethyl ether, essentially indistinguishable from those of the 77 K EPR spectrum of the fully delocalized mixed-valence complex **37**, exhibits high rhombicities with three principal g values of 2.17, 2.05, and 2.02, which are different from those of the mononuclear d^7 Ni(III) complex **29** [37]. These results implicate that complex **38** may exist as the delocalized mixed-valence [Ni(II)–Ni(III)] complex. The lengthening of the Ni···Ni distance was expected to be driven by reduction of complex **37**; the reduction of complex **37** by 1 equiv of KC_8 yielded a dianionic $[Ni_2(P(o\text{-}C_6H_3\text{–}3\text{-}SiMe_3\text{–}2\text{-}S)_3)_2]^{2-}$ (**39**) with a Ni···Ni distance of 3.186 Å (Scheme 13e) [39].

As shown in Scheme 14, the geometrical (coordination environment) change from distorted square pyramidal to distorted square planar (i.e., from butterfly structure of the [Ni(μ-S)$_2$Ni] core to the diamond shape of the [NiS$_2$Ni] core) occurs upon going from a [d^7 Ni(III)–d^7 Ni(III)] electronic structure of complex **36** to a fully delocalized mixed-valence [d^8 Ni(II)–d^7 Ni(III)] electronic structure of complex **37**. In particular, the different oxidation levels of the [PS$_3$Ni–NiPS$_3$] units between complexes **36** and **37** reflect the distinctly different Ni···Ni distances, 2.603(1) Å for complex **36** and 2.829(1) Å for complex **37**, to reach the optimum electron density of the [PS$_3$Ni–NiPS$_3$] core of complexes **36** and **37**. The electronic perturbation from the sulfur methylation of complex **37** triggers the stronger Ni···Ni interaction and the geometrical rearrangement from the diamond shape of the [NiS$_2$Ni] core to the butterfly structure of [Ni(μ-S)$_2$Ni], resulting in the formation of complex **38** (Scheme 14). Presumably, the shortening of the Ni···Ni distance of complex **38** (vs complex **37**) was employed to reimburse the electron deficiency induced by methylation, neutralizing the thiolate negative charge. Also, the geometrical change of the nickel centers from distorted tetrahedral to square planar and the

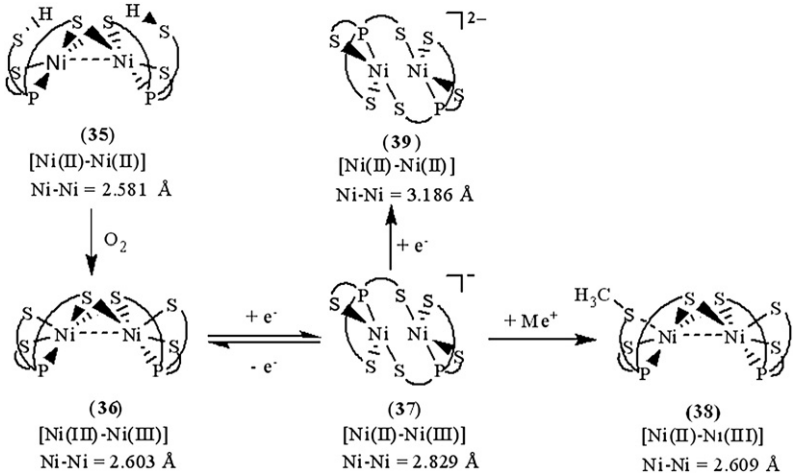

Scheme 14.

lengthening of the Ni···Ni distance (from 2.581 to 3.186 Å) occur upon going from a neutral [Ni(II)-Ni(II)] electronic structure of complex **35** to a dianionic [Ni(II)Ni(II)] electronic structure of complex **39**. Such geometrical differences as determined by the nickel oxidation state in complex **36** versus that in complex **37** and determined by the coordinated ligands in complex **37** versus those in complex **38** (or in complex **35** versus those in complex **39**) demand ligands capable of matching the geometrical requirement of the $[Ni(SR)_2Ni]$ unit as well as maintaining the preferred coordination number of the nickels (Scheme 14). Obviously, the presence/absence of Ni···Ni interaction in cooperation with the geometrical rearrangement were employed by dinuclear complexes **35**–**39** as an efficient tool to reach an optimum electronic condition to stabilize the dinuclear nickel complexes [39]. These results unambiguously illustrate the aspects of how a coordinated ligand and the electronic states (oxidation states) of two nickel centers function to trigger the geometrical rearrangement, to promote the stability of the dinuclear nickel complexes via the Ni···Ni interaction. This result may provide some clues to rationalize the oxidized-form active-site structure of [NiFe] hydrogenases, a heterobimetallic $(S_{cys})_2Ni(\mu\text{-}S_{cys})_2(\mu\text{-}X)Fe(CO)(CN)_2$ ($X = O^{2-}$, HO^{2-}, OH^-) with the butterfly structure of the $[Ni(\mu\text{-}S_{cys})_2$–Fe] core and a Ni···Fe distance of 2.6 Å.

5. Conclusion

Recently, the major progress has been made in solving the active-site structures of [NiFe]/[Fe] hydrogenases by high-resolution single-crystal X-ray diffraction and in elucidating the ways that hydrogenases catalyze reversible hydrogen oxidation [1–12]. Extensive spectroscopic experiments have been performed, as a background for the subsequent modeling studies [1–12]. For the past few years, our studies on the iron(II)–thiolate cyanocarbonyls, the mononuclear/dinuclear nickel(III)–thiolate complexes and the mononuclear nickel(II)–thiolate complexes with pendant thiol have led to the interesting results related to the structure, reactivity and spectroscopic properties of the iron and nickel centers of the active site of [NiFe]/[Fe] hydrogenases.

Acknowledgements

We gratefully acknowledge financial support from the National Science Council of Taiwan.

References

[1] (a) A. Volbeda, M.-H. Charon, C. Piras, E.C. Hatchikian, M. Frey, J.C. Fontecilla-Camps, Nature 373 (1995) 580;
(b) A.L. de Lacey, E.C. Hatchikian, A. Volbeda, M. Frey, J.C. Fontecilla-Camps, V.M. Fernandez, J. Am. Chem. Soc. 119 (1997) 7181;
(c) R.P. Happe, W. Roseboom, A.J. Pierik, S.P.J. Albracht, K.A. Bagley, Nature 385 (1997) 126;
(d) A.J. Pierik, W. Roseboom, R.P. Happe, K.A. Bagley, S.P.J. Albracht, J. Biol. Chem. 274 (1999) 3331;
(e) R.H. Holm, P. Kennepohl, E.I. Solomon, Chem. Rev. 96 (1996) 2239.

[2] (a) Z. Gu, J. Dong, C.B. Allan, S.B. Choudhury, R. Franco, J.J.G. Moura, I. Moura, J. LeGall, A.E. Przybyla, W. Roseboom, S.P.J. Albracht, M.J. Axley, R.A. Scott, M.J. Maroney, J. Am. Chem. Soc. 118 (1996) 11155;
(b) G.J. Colpas, R.O. Day, M.J. Maroney, Inorg. Chem. 31 (1992) 5053;
(c) L.M. Robert, P.A. Lindahl, J. Am. Chem. Soc. 117 (1995) 2565.

[3] (a) Y. Nicolet, C. Piras, P. Legrand, C.E. Hatchikian, J.C. Fontecilla-Camps, Structure 7 (1999) 13;
(b) A.L. de Lacey, C. Stadler, C. Cavazza, E.C. Hatchikian, V.M. Fernandez, J. Am. Chem. Soc. 122 (2000) 11232.

[4] J.W. Peters, W.N. Lanzilotta, B.J. Lemon, L.C. Seefeldt, Science 282 (1998) 1853.

[5] (a) A.J. Pierik, M. Hulstein, W.R. Hagen, S.P.J. Albracht, Eur. J. Biochem. 258 (1998) 572;
(b) P.J. Van Dam, E.J. Reijerse, W.R. Hagen, Eur. J. Biochem. 248 (1997) 355;
(c) C.V. Popescu, E. Münck, J. Am. Chem. Soc. 121 (1999) 7877.

[6] (a) C.-H. Lai, W.-Z. Lee, M.L. Millar, J.H. Reibenspies, D.J. Darensbourg, M.Y. Darensbourg, J. Am. Chem. Soc. 120 (1998) 10103;
(b) D.J. Darensbourg, J.H. Reibenspies, C.-H. Lai, W.-Z. Lee, M.Y. Darensbourg, J. Am. Chem. Soc. 119 (1997) 7903;
(c) C.A. Boyke, J.I. van der Vlugt, T.B. Rauchfuss, S.R. Wilson, G. Zampella, L. De Gioia, J. Am. Chem. Soc. 127 (2005) 11010.

[7] (a) E. Garcin, X. Vernede, E.C. Hatchikian, A. Volbeda, M. Frey, J.C. Fontecilla-Camps, Structure 7 (1999) 557;
(b) A. Volbeda, E. Garcin, C. Piras, A.L. De Lacey, V.M. Fernandez, E.C. Hatchikian, M. Frey, J.C. Fontecilla-Camps, J. Am. Chem. Soc. 118 (1996) 12989.

[8] A. Volbeda, L. Martin, C. Cavazza, M. Matho, B.W. Faber, W. Roseboom, S.P.J. Albracht, E. Garcin, M. Rousset, J.C. Fontecilla-Camps, J. Biol. Inorg. Chem. 10 (2005) 239.

[9] (a) Y. Higuchi, T. Yagi, N. Yasuoka, Structure 5 (1997) 1671;
(b) Y. Higuchi, H. Ogata, K. Miki, N. Yasuoka, T. Yagi, Structure 7 (1999) 549;
(c) H. Ogata, Y. Mizoguchi, N. Mizuno, K. Miki, S.-I. Adachi, N. Yasuoka, T. Yagi, O. Yamauchi, S. Hirota, Y. Higuchi, J. Am. Chem. Soc. 124 (2002) 11628;
(d) S. Foerster, M. Stein, M. Brecht, H. Ogata, Y. Higuchi, W. Lubitz, J. Am. Chem. Soc. 125 (2003) 83;
(e) H. Ogata, S. Hirota, A. Nakahara, H. Komori, N. Shibata, T. Kato, K. Kano, Y. Higuchi, Structure 13 (2005) 1635.

[10] M. Rousset, Y. Montet, B. Guigliarelli, A. Forget, M. Asso, P. Bertrand, J.C. Fontecilla-Camps, E.C. Hatchikian, Proc. Natl. Acad. Sci. U.S.A. 95 (1998) 11625.

[11] (a) M.J. Maroney, G. Davidson, C.B. Allan, J. Figlar, Struct. Bond. 92 (1998) 1;

(b) M.M. Stein, W. Lubitz, Curr. Opin. Chem. Biol. 6 (2002) 243;
(c) S.E. Lamle, S.P. Albracht, F.A. Armstrong, J. Am. Chem. Soc. 127 (2005) 6595.
[12] (a) M. Haumann, A. Porthum, T. Buhrke, P. Liebisch, W. Meyer-Klaucke, B. Friedrich, H. Dau, Biochemistry 42 (2003) 11004;
(b) M. Brecht, M.V. Gastel, T. Buhrke, B. Friedrich, W. Lubitz, J. Am. Chem. Soc. 125 (2003) 13075.
[13] (a) J.K. Ruff, Inorg. Chem. 8 (1969) 86;
(b) S.A. Goldfield, K.N. Raymond, Inorg. Chem. 13 (1974) 770.
[14] W.-F. Liaw, N.-H. Lee, C.-H. Chen, C.-M. Lee, G.-H. Lee, S.-M. Peng, J. Am. Chem. Soc. 122 (2000) 488.
[15] W.-F. Liaw, C.-H. Chen, G.-H. Lee, S.-M. Peng, Organometallics 17 (1998) 2370.
[16] C.-M. Lee, G.-Y. Lin, C.-H. Hsieh, C.-H. Hu, G.-H. Lee, S.-H. Peng, W.-F. Liaw, J. Chem. Soc., Dalton Trans. (1999) 2393.
[17] W.-F. Liaw, J.-H. Lee, H.-B. Gau, C.-H. Chen, S.-J. Jung, C.-H. Hung, W.-Y. Chen, C.-H. Hu, G.-H. Lee, J. Am. Chem. Soc. 124 (2002) 1680.
[18] (a) G. Davidson, S.B. Choudhury, Z. Gu, K. Bose, W. Roseboom, S.P.J. Albracht, M.J. Maroney, Biochemistry 39 (2000) 7468;
(b) E.C. Hatchikian, A.S. Traore, V.M. Fernandez, R. Cammack, Eur. J. Biochem. 187 (1990) 635;
(c) M.Y. Darensbourg, E.J. Lyon, J.J. Smee, Coord. Chem. Rev. 206 (2000) 533.
[19] (a) C.-H. Chen, Y.-S. Chang, C.-Y. Yang, T.-N. Chen, C.-M. Lee, W.-F. Liaw, Dalton Trans. (2004) 137;
(b) T.B. Rauchfuss, S.M. Contakes, S.C.N. Hsu, M.A. Reynold, S.R. Wilson, J. Am. Chem. Soc. 123 (2001) 6933.
[20] (a) W.-F. Liaw, W.-T. Tsai, H.-B. Gau, C.-M. Lee, S.-Y. Chou, W.-Y. Chen, G.-H. Lee, Inorg. Chem. 42 (2003) 2783;
(b) J.I. van der Vlug, T.B. Rauchfuss, C.M. Whaley, S.R. Wilson, J. Am. Chem. Soc. 127 (2005) 16012;
(c) M. Razavet, S.C. Davies, D.L. Hughes, C.J. Pickett, Chem. Commun. (2001) 847;
(d) M. Razavet, S.J. Borg, S.J. George, S.P. Best, S.A. Fairhurst, C.J. Pickett, Chem. Commun. (2002) 700.
[21] J. Jiang, S.A. Koch, Angew. Chem., Int. Ed. 40 (2001) 2629.
[22] (a) W.-F. Liaw, C.-Y. Chiang, G.-H. Lee, S.-M. Peng, C.-H. Lai, Y.M. Darensbourg, Inorg. Chem. 39 (2000) 480;
(b) D. Sellmann, F. Geipel, F. Lauderbach, F.W. Heinemann, Angew. Chem. Int. Ed. 41 (2002) 632;
(c) C.-H. Lai, J.H. Reibenspies, M.Y. Darensbourg, Angew. Chem. Int. Ed. 35 (1996) 2390;
(d) A.C. Marr, D.J.E. Spencer, M. Schröder, Coord. Chem. Rev. 219–221 (2001) 1055;
(e) S.C. Davies, D.J. Evans, D.L. Hughes, S. Longhurst, J.R. Sanders, J. Chem. Soc., Chem. Commun. (1999) 1935;
(f) Z. Li, Y. Ohki, K. Tatsumi, J. Am. Chem. Soc. 127 (2005) 8950;
(g) W. Zhu, A.C. Marr, Q. Wang, F. Neese, D.J.E. Spencer, A.J. Blake, P.A. Cooke, C. Wilson, M. Schröder, Proc. Natl. Acad. Sci. U.S.A. 102 (2005) 18280.
[23] J.H. Enemark, R.D. Feltham, Coord. Chem. Rev. 13 (1974) 339.
[24] D.J. Darensbourg, T.J. Decuir, N.W. Stafford, J.B. Robertson, J.D. Draper, J.H. Reibenspies, A. Kathó, F. Joó, Inorg. Chem. 36 (1997) 4218.
[25] W.-F. Liaw, C.-H. Lai, C.-K. Lee, G.-H. Lee, S.-M. Peng, J. Chem. Soc. Dalton Trans. (1993) 2421.
[26] W.-F. Liaw, Y.-C. Horng, D.-S. Ou, C.-Y. Chiang, G.-H. Lee, S.-M. Peng, J. Am. Chem. Soc. 119 (1997) 9299.
[27] P. Stavropoulos, M.C. Muetterties, M. Carrié, R.H. Holm, J. Am. Chem. Soc. 113 (1991) 8485.
[28] C.A. Marganian, H. Vazir, N. Baidya, M.M. Olmstead, P.K. Mascharak, J. Am. Chem. Soc. 117 (1995) 1584.
[29] D.H. Nguyen, H.-F. Hsu, M. Millar, S.A. Koch, C. Achim, E.L. Bominaar, E. Münck, J. Am. Chem. Soc. 118 (1996) 8963.
[30] W.-F. Liaw, C.-H. Chen, C.-M. Lee, G.-H. Lee, S.-M. Peng, J. Chem. Soc. Dalton Trans. (2001) 138.
[31] L.L. Efros, H.H. Thorp, G.W. Brudvig, R.H. Crabtree, Inorg. Chem. 31 (1992) 1722.
[32] C.-M. Lee, C.-H. Chen, S.-C. Ke, G.-H. Lee, W.-F. Liaw, J. Am. Chem. Soc. 126 (2004) 8406.
[33] E. Block, G. Ofori-Okai, J. Zubieta, J. Am. Chem. Soc. 111 (1989) 2327.
[34] M.Y. Darensbourg, W.-F. Liaw, C.G. Riordan, J. Am. Chem. Soc. 111 (1989) 8051.
[35] C.-H. Chen, G.-H. Lee, W.-F. Liaw, Inorg. Chem. 45 (2006) 2307.
[36] C.-M. Lee, Y.-L. Chuang, C.-Y. Chiang, G.-H. Lee, W.-F. Liaw, Inorg. Chem. 45 (2006) 10895.
[37] (a) M. Carepo, D.L. Tierney, C.D. Brodino, T.C. Yang, A. Pamplona, J. Telser, I. Moura, J.J.G. Moura, B.M. Hoffman, J. Am. Chem. Soc. 124 (2002) 281;
(b) S.P.J. Albracht, Biochim. Biophys. Acta 1188 (1994) 167;
(c) J.W. van der Zwaan, J.M.C.C. Coremans, E.C.M. Bouwens, S.P.J. Albracht, Biochim. Biophys. Acta 1041 (1990) 101.
[38] P.R. Alburquerque, A.R. Pinhas, J.A.K. Bauer, Inorg. Chim. Acta 298 (2000) 239.
[39] C.-M. Lee, T.-W. Chiou, H.-H. Chen, C.-Y. Chiang, T.-S. Kuo, W.-F. Liaw, Inorg. Chem. 46 (2007) 8913.